

Growth mechanism and multiphoton-induced photoluminescence of crownlike zinc oxide

G. P. Zhu · C. X. Xu · J. Zhu · M. H. Wang

Received: 12 April 2010/Accepted: 20 October 2010/Published online: 11 November 2010
© Springer Science+Business Media, LLC 2010

Abstract A crownlike zinc oxide crystal composed of a hexagonal cap and a towerlike shaft was synthesized by vapor-phase transport method. Based on vapor–liquid–solid and vapor–solid mechanism, the growth model of the crystal was proposed. Under the excitation of pulse laser with 1150-nm wavelength, strong ultraviolet emission at 388 nm was observed. The peak position and the relationship between the emission intensity and excitation intensity demonstrated that the ultraviolet photoluminescence was induced by three-photon absorption. The photoluminescence characteristic of the sample was investigated.

Introduction

In recent years, nanostructural ZnO has attracted a great interest because of its rich morphology and potential multifunctional applications. A considerable endeavor has been paid to obtain desirable ZnO nanostructures by controlling growth condition, and various morphologic ZnO nanostructures have been fabricated by different methods, including chemical vapor deposition [1, 2], oxidizing granular Zn films [3], template-oriented growth [4], supercritical hydrothermal synthesis [5], metalorganic

vapor-phase epitaxy [6, 7], and low-temperature solution method [8], etc. Meanwhile, various optoelectronic functions of nanostructural ZnO have also been revealed, such as UV laser [9, 10], field effect transistor [11], sensor [12, 13], and nanogenerator [14]. In addition, ZnO optical nonlinearity effects, such as second and third harmonic generations, two-photon absorption and photoluminescence have been found in ZnO thin film [15–17], ZnO microtubes, and ZnO nanowires [18, 19]. All these nonlinear effects have shown potential applications of ZnO in optical limiting [20], all-optical switching [21], and optical data storage [22]. However, three-photon-induced photoluminescence (TPPL) in ZnO nanostructures has rarely been seen. In this article, a crownlike ZnO nanostructure composed of a hexagonal cap and a towerlike shaft was synthesized by vapor-phase transport method. Under the excitation of pulse laser with 1150-nm wavelength, the UV TPPL was observed, and the photoluminescence characteristic of the sample was discussed.

Experimental methods

The ZnO sample was produced in a tube furnace. A small quartz boat filled with high purity Zn powders was placed in a slender quartz tube with both ends open. A strip of silicon wafer with (100) plane was put into quartz tube downstream from the boat as a deposition substrate. The furnace chamber was heated at a rate of 20 °C/min after the quartz tube had been inserted it. Meanwhile, a mechanical pump was installed to exhaust air in the chamber, and the vapor pressure was maintained 50 kPa during the whole growth process. When the source region was raised to 750 °C, nitrogen was introduced into the furnace chamber with a flux rate of 200 sccm (standard cubic centimeter per

G. P. Zhu (✉)
School of Physics and Electronic Information,
HuaiBei Normal University, HuaiBei, China
e-mail: guang.pingzhu@yahoo.com.cn

C. X. Xu · J. Zhu
Advanced Photonics Center, School of Electronic Science
and Engineering, Southeast University, Nanjing, China

M. H. Wang
Faculty of Electronic and Electrical Engineering,
Huaiyin Institute of Technology, HuaiAn, China

minute). During 30-min growth time, the source region temperature was kept at 750 °C, and the substrate temperature at about 500 °C. A scanning electron microscopy (SEM) was employed to examine the sample morphology. The sample microstructure was characterized by X-ray diffraction (XRD) and the high-resolution transmission electron microscopy (HRTEM). A femtosecond pulse laser at 1150 nm generated from an optical parametric oscillator (repetition frequency 1000 Hz, pulse duration 150 fs) was used as excitation light source. The excitation beam was focused into a spot with a diameter of about 100 μm by a convex lens, and the emission signal was recorded by a fiber-coupled optical multi-channel analyzer (OMA). All the measurements were carried out at room temperature.

Results and discussion

The XRD pattern of the sample is illustrated in Fig. 1. All diffraction peaks match the indexes of the wurtzite ZnO with lattice constants $a = 0.325$ nm and $c = 0.521$ nm. The strongest (0002) peak of the sample shows a preferred growth orientation along the c -axis.

The low-magnification SEM image of the sample in Fig. 2a indicates its high yield. The SEM images with medium and high magnification in Fig. 2b and c illustrate that each product presents a novel crownlike morphology composed of two parts: (1) a towerlike shaft with a hexagram cross section and a varied diameter of several micrometers to several hundred nanometers from the bottom to the top, and (2) a hexagonal disk with about 1-μm diameter capping on the shaft top. Figure 2d is the field emission SEM image of a selected product. A dark hexagonal spot can obviously be seen on the disklike cap. The HRTEM image of a shaft in Fig. 3a clearly shows the lattice fringes. The 0.26-nm d -spacing matches (0001) interspacing of the wurtzite ZnO; this indicates that the

shaft grew mainly along [0001] consistent with the XRD pattern. Figure 3b is the HRTEM image of a disklike cap viewed from [0001] direction. It can be seen that the atoms arrange regularly to form a sixfold symmetric projected structure. The 0.28-nm d -spacing between any two adjacent lattice fringes along six symmetric directions corresponds to the interspacing of $\{10\bar{1}0\}$ of the wurtzite ZnO. This indicates that the disklike cap is formed by (0001) plane closed by six symmetric $\{10\bar{1}0\}$ similar to the ZnO nanodisks as reported by Xu et al. [23].

The ZnO nanostructures—similar to our crownlike ZnO, such as nanonail and crown-capped nanotrapod—have been synthesized [24–26], and the corresponding growth mechanisms were proposed. For example, Lao et al. [24] attributed the ZnO nanonail formation to a preferential growth chance of the nanorod top relative to the bottom, while Zhang et al. [25] proposed that the nanonail formation originated from an abrupt variation of Zn–O concentration at the last growth stage. In the case of this study, the crownlike ZnO shape distinguishes from above nail-like nanostructures, and so the growth mechanism of the latter should also be different. From the SEM images in Fig. 2, it can be seen that the ZnO products growth involved two stages: (1) the towerlike shaft growth and (2) the disklike cap formation.

Because no catalyst was introduced in this experiment, the shaft growth along [0001] should be controlled by self-catalyst vapor–liquid–solid (V–L–S) mechanism. The vapor-phase Zn atoms from the source region are first liquefied into zinc droplets on the substrate. These droplets absorb vapor-phase growth units such as zinc and oxygen atoms or zinc suboxide in the atmosphere to form ZnO nucleus from which the shafts begin to grow along [0001]. It is interesting to note that the shaft exhibits hexagram, which is not often observed in rodlike ZnO. The ZnO nanorod generally presents hexagon with $\{10\bar{1}0\}$ as six sides at a lower supersaturation ratio, because the growth velocity along $\langle 11\bar{2}0 \rangle$ is larger than that along $\langle 10\bar{1}0 \rangle$ in this case. However, at a higher supersaturation ratio, ZnO nanorod possibly grows more rapidly along $\langle 10\bar{1}0 \rangle$ than along $\langle 11\bar{2}0 \rangle$, which has been confirmed by another experiment of the authors. Figure 4a is the SEM image of the ZnO nanorods fabricated by carbon thermal reductive reaction with ZnO powders and graphite powders as source materials at 1150 °C temperature in air, and the corresponding growth temperature is about 700 °C. It can be seen that the upper part of a nanorod presents hexagon, but its lower part exhibits hexagram, and the six sides of the hexagon are clearly formed by flattening of the six edges of the hexagon. Because the upper part of the nanorod grew in the last stage, the six sides of the hexagon should be $\{10\bar{1}0\}$ because of a lower supersaturation ratio. The

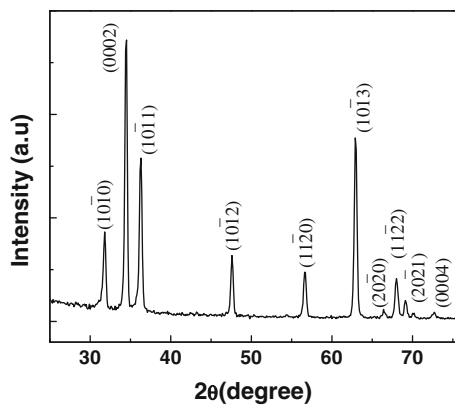


Fig. 1 The XRD pattern of the crownlike ZnO

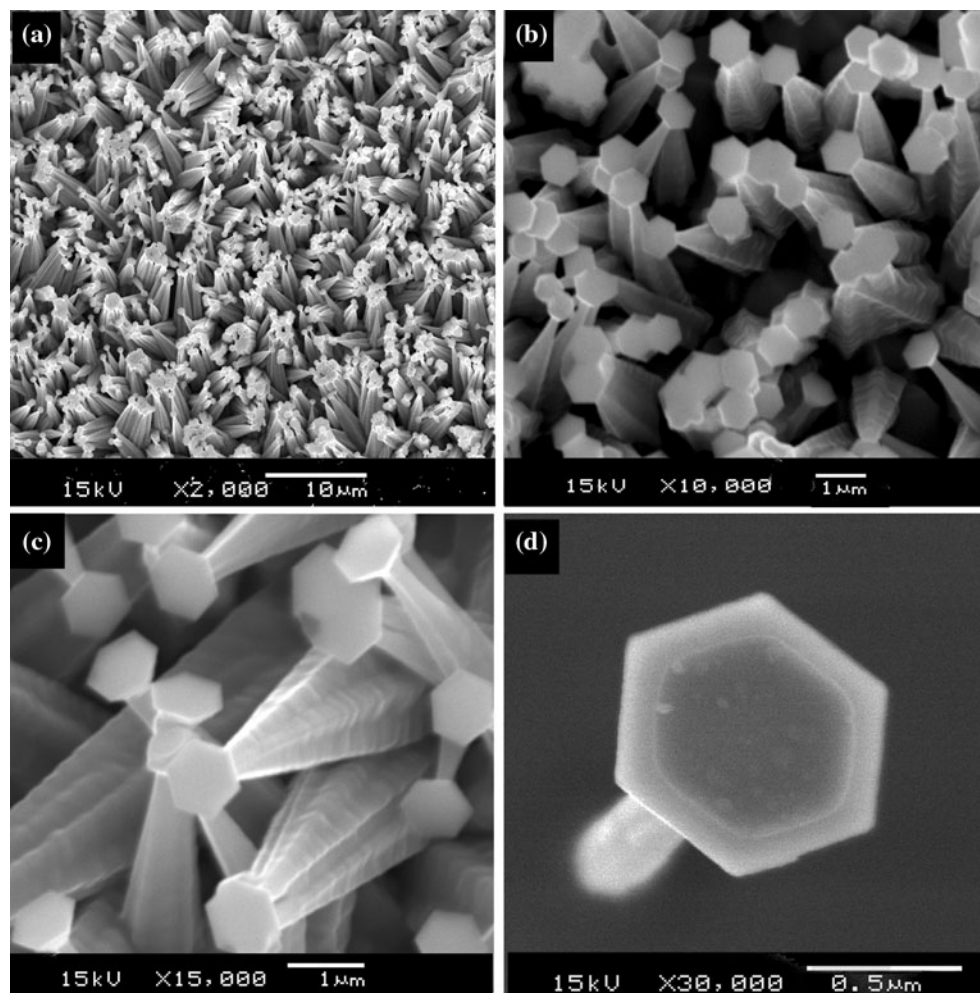
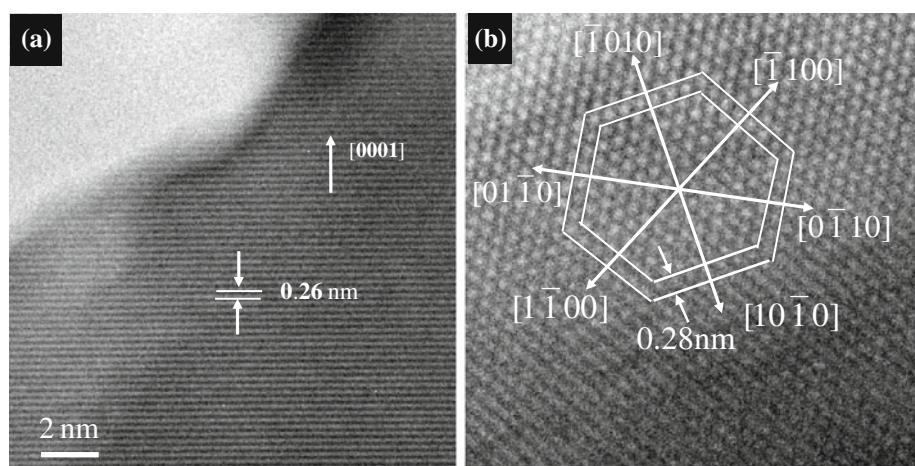


Fig. 2 The SEM images of the crownlike ZnO with low (**a**), medium (**b**, **c**) and high (**d**) magnifications

Fig. 3 HRTEM images of the shaft and the disklike cap of a crownlike ZnO



schematic variation process of the nanorod shape is shown in Fig. 4b. At the early growth stage, owing to a higher supersaturation ratio, the nanorod grows faster along $\langle 10\bar{1}0 \rangle$ than along $\langle 11\bar{2}0 \rangle$, and this results in a hexagram cross section of the nanorod, in which the six angles

correspond to $\langle 10\bar{1}0 \rangle$ directions. With decrease of supersaturation ratio in growth region, the nanorod growth velocity along $\langle 10\bar{1}0 \rangle$ relative to $\langle 11\bar{2}0 \rangle$ will reduce, and thus its six angles will become blunt. When the supersaturation ratio lowers to a proper level, the growth velocity

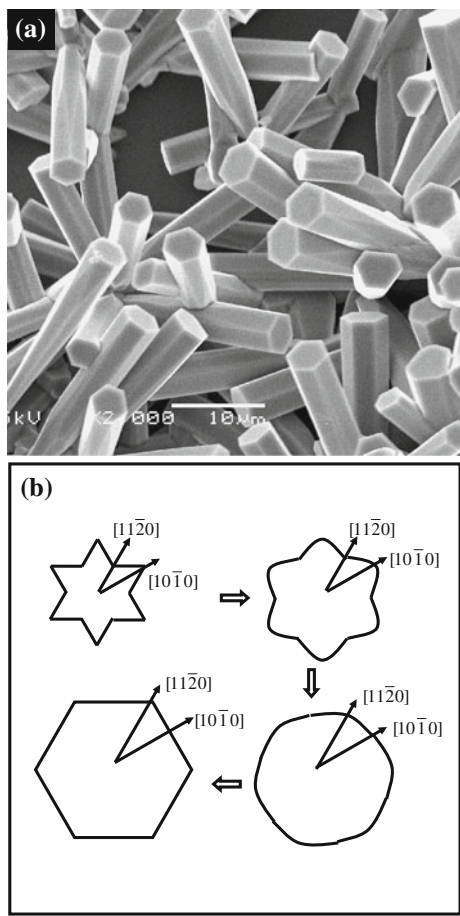


Fig. 4 **a** The SEM image of ZnO nanorods, **b** the evolvement of the ZnO nanorod cross section with growth process

along $\langle 11\bar{2}0 \rangle$ will exceed that along $\langle 10\bar{1}0 \rangle$, and the six angles of the nanorod will gradually flatten and finally form a hexagonal cross section with $\{10\bar{1}0\}$ as six sides. Based on above discussion, the hexagram shaft formation of the crownlike ZnO can be attributed to a higher supersaturation ratio.

It is noted that the shaft presents a clear towerlike structure, and each layer has a height of about 20 nm. The ZnO nanostructures with similar morphology have been reported [27–29], but the growth mechanism is still unclear. The towerlike shaft was impossibly formed by pure V–L–S mechanism. In that case, the shaft should have near same diameter with the catalyst liquid droplet from bottom to top, so the towerlike structure should be caused by transverse growth of the shaft controlled by vapor–solid (V–S) mechanism. In vapor-phase condition, the V–S-controlled crystal growth is generally difficult if no defects (such as screw dislocation or twin-crystal) provide growth steps. However, in our case, no screw dislocations or twin-crystals are observed from the HRTEM image in Fig. 3a, and so it is believed that the growth steps can first be provided by the

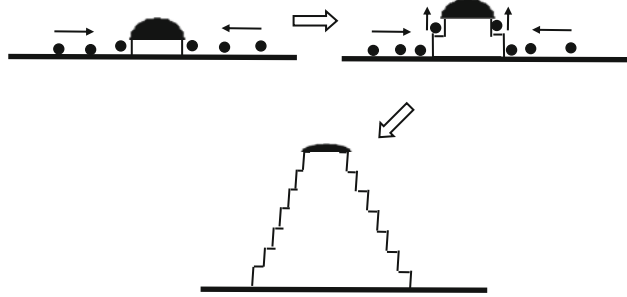


Fig. 5 The diagram illustrating the towerlike shaft formation

corners formed by the substrate and nuclei (shown in Fig. 5). In ZnO nucleation process, the growth step is simultaneously generated by the nuclei and the substrate. Thus, when the shaft grows, the growth units falling on the substrate will transfer to the steps and move upward along the shafts, and some of them will be adsorbed and enter crystal lattice sites. Because the transfer distance of growth units is limited, the first-order step will be formed on the shaft when the shaft grows to a certain length. Similarly, the second-order step will be formed by the first-order step on the shaft. Owing to a gradually decreasing transverse growth time of the steps from bottom to top, the shaft finally will present a towerlike morphology.

The second growth stage is the cap formation. It is well known that the supersaturation ratio is most main factor of crystal growth, so the system should still have an appropriate vapor pressure to supply the cap growth in this stage. This also implies that the longitudinal growth stop of the shaft was not mainly caused by the decrease of supersaturation ratio. Based on above discussion, and combining the SEM image of the cap in Fig. 2d, we believe that the change of catalyst shape can be main factor suppressing the $[0001]$ growth of the shaft. In the first growth stage, the area of the shaft top will gradually increase because of transverse growth. In this situation, the curvature of catalyst droplet will become smaller and smaller because of surface strain between it and the shaft top; therefore, its adsorbability to the growth units will generally reduce. When the catalyst droplet finally gets flat enough, it can no longer adsorb sufficient growth units, and the shaft growth along $[0001]$ will stop (shown in Fig. 5). The dark spot covering the cap (Fig. 2d) implies the existence of the liquid-phase catalyst during the growth process. However, the sides of the top can still grow to some extent, and this will lead the growth units to diffuse from the shaft top to the sides. This transfer will lead to a preferential transverse growth of the shaft top relative to other parts. As a result, a disk will be formed from the shaft top. Because the supersaturation ratio is smaller in this growth stage, the cap presents hexagon with $\{10\bar{1}0\}$ as six sides.

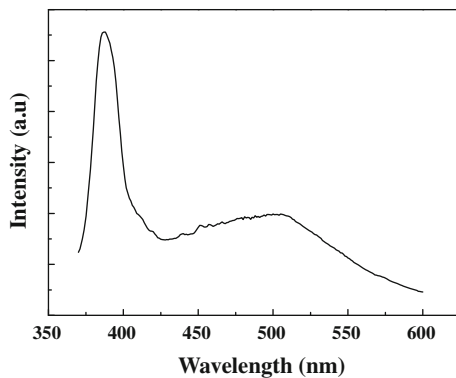


Fig. 6 PL spectrum of the crownlike ZnO excited by Xe lamp at 350 nm

Under the excitation of 350-nm light from Xe lamp, the photoluminescence (PL) spectrum of the ZnO products is shown in Fig. 6. It is composed of two emission bands: a stronger narrow UV band at 388 nm, and a weaker broad green band peaked at 510 nm. The UV emission of ZnO is generally attributed to near-band edge emission, but the origin of green emission is still controversial. Jayakumar et al. investigated the green emissions of the ZnO nanorods fabricated by solvothermal method and treated in hydrogen, vacuum, and in air at 400 °C and room temperature, and attributed the green emission to Zn vacancies [30]. Djurišić et al. observed the green emission in tetrapod structures fabricated by thermal evaporation of zinc powders in air, dry, and humid argon flow as well as nitrogen flow, and proposed that the green emission could originate from surface defects [31]. In addition, other mechanisms, such as singly ionized oxygen vacancy [32], copper impurities [33], antisite oxygen [34], donor–acceptor complexes [35], and zinc interstitials [36], were also used to explain green emission by some authors. These different explanations indicate that the green emission is likely to originate from more than one defect, these defects can depend on the given preparation methods and post-treatment process.

Figure 7a shows the PL spectra of the products excited by 1150-nm femtosecond laser under a different power. It can be seen that all spectra contain a UV band peaked at 388 nm, and a visible band centered at 575 nm. Because the excitation wavelength is more than two times but less than three times of the peak wavelength, it is believed that the UV emission can be generated from TPPL process (shown in the inset of Fig. 7a).

The TPPL originates from three-photon absorption. An electron excited by intense light field probably transits from a lower energy level to a higher energy level by simultaneously absorbing three photons. When this electron transits to low energy levels, it can generate spontaneous emission, namely TPPL. The TPPL probability

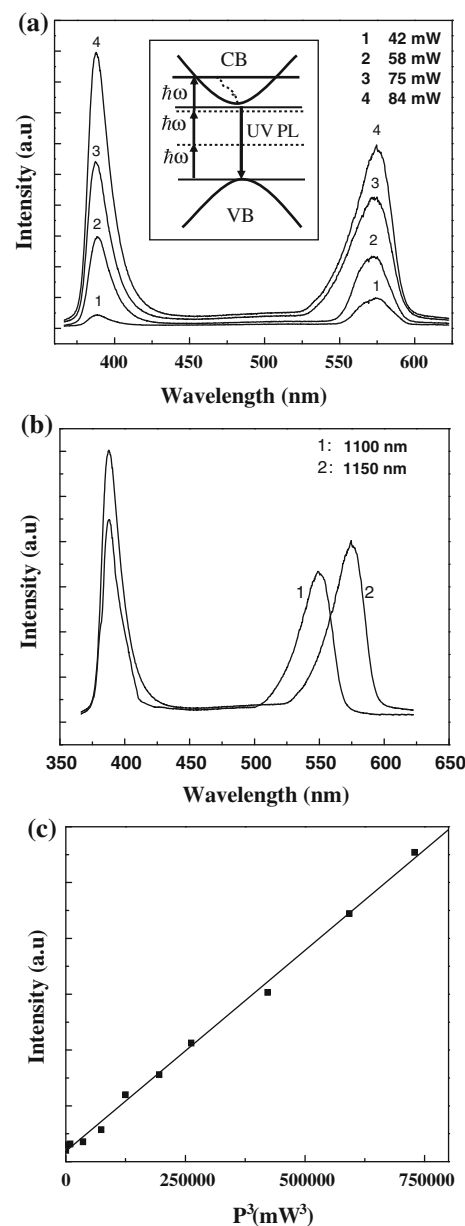


Fig. 7 Three-photon-induced PL spectra excited by 1150-nm femtosecond laser with various powers (a), the UV PL spectral at the different excitation wavelength (b), and UV emission intensity variation vs the cube of excitation power (c), the *inset* of a is the schematic diagram of TPPL process

mainly depends on the three-photon absorption probability, which mechanism can be explained by solving the time-dependent Schrödinger equation using the third-order perturbation theory. For a semiconductor in light field, the time-dependent Schrödinger equation of an electron is expressed as follows:

$$\hat{H}\psi = i\hbar \frac{\partial}{\partial t} \psi \quad (1)$$

where \hat{H} is the Hamilton operator of the electron, and

$$\hat{H} = \frac{1}{2m} \left(\hat{\vec{p}} + \frac{e}{c} \vec{A} \cdot \hat{\vec{p}} \right)^2 + V(r) - e\varphi \quad (2)$$

$\hat{\vec{p}}$ is momentum operator of the electron, \vec{A} and φ are, respectively, the vector and scalar potentials of electromagnetic field, and $V(r)$ is the electron potential energy in crystal field.

Using coulomb criterion $\nabla \cdot \vec{A} = 0$, and $\varphi = 0$, \hat{H} can be expressed as

$$\hat{H} = \hat{H}_0 + \hat{H}'_1 + \hat{H}'_2 \quad (3)$$

where

$$\hat{H}_0 = \frac{1}{2m} \hat{\vec{p}}^2 + V(r) \quad (4)$$

is the Hamilton operator of the electron without perturbation of light field, and

$$\hat{H}'_1 = \frac{e}{mc} \vec{A} \cdot \hat{\vec{p}} \quad (5)$$

$$\hat{H}'_2 = \frac{e^2}{2mc} \vec{A} \cdot \vec{A} \quad (6)$$

are, respectively, the interactional Hamilton operators of the light field and the electron, \hat{H}'_1 , \hat{H}'_2 is far less than \hat{H}_0 , and $H'_2 \ll H'_1$. In the case of third-order approximation, H'_2 effect in Eq. 1 can be omitted.

Using the third-order time-dependent perturbation theory to Eq. 1, the total three-photon transition probability of the electron from a valence band v to a conduction band c can be written as follows [37]:

$$W_3 = \frac{2\pi}{\hbar} \int \frac{d^3k}{(2\pi)^3} \times \sum_n \sum_m \frac{H'_{vm} H'_{mn} H'_{nc} \delta[E_{vc}(\vec{k}) - 3\hbar\omega]}{[E_{mv}(\vec{k}) - \hbar\omega][E_{mn}(\vec{k}) - 2\hbar\omega]} \quad (7)$$

where

$$H'_{nm} = \int \psi_n^* \hat{H}'_1 \psi_m dv = \int_v \psi_n^* \left(\frac{e}{mc} \vec{A} \cdot \hat{\vec{p}} \right) \psi_m dv$$

and the indices m and n refer to the intermediate bands, ψ_m is the Bloch wave function of m band, E_{nm} is the energy difference between band n and band m, and \vec{k} is wave-vector. From Eq. 7, it can be deduced that three-photon absorption is usually realized by a series of intermediate state, and only when $E_c - E_v \approx 3\hbar\omega$, the absorption has a larger probability. The most main characteristic of three-photon absorption is that its transition probability is proportional to cube of excitation light intensity.

According to discussion, the TPPL mechanism in the case of this study case is explained as follows: an electron in the valence band (VB) simultaneously absorbs three photons by intermediate energy bands and transits to the conduction band (CB), then relaxes to an exciton state near

the band edge, and finally generates UV emission by exciton recombination.

The visible peak at 575 nm is attributed to the second harmonic generation (SHG) of the excitation light. In order to further confirm it, we compared the two PL spectra (shown in Fig. 7b) at different excitation wavelengths (1150 and 1100 nm) under 84-mW excitation power. It is clear that the UV peak still keeps at 388 nm for 1100 nm excitation wavelength, but the visible peak shifts to 550 nm. This indicates that the UV peak is undoubtedly TPPL (it can also be demonstrated by the approximately linear relation between the UV emission intensity and cube of excitation power in Fig. 7c), and the visible band originates from SHG of the excitation light. It is noted that the UV emission intensity increases more rapidly relative to the visible emission with excitation power increase as can be seen from Fig. 7a. This can be attributed to the difference in the dependencies between TPPL intensity and SHG intensity on the excitation intensity. TPPL intensity is proportional to cube of excitation intensity, whereas SHG intensity depends on square of excitation intensity. It is necessarily mentioned that the SHG linewidth (about 28 nm) is far more than the excitation light linewidth (about 14 nm) observed in this study, which can be caused by the broadening of the visible TPPL that originated from defect emission.

Recently, Dong et al. [38] reported two-photon-induced luminescence of ZnO nanowires with 800 nm fs laser as excitation light source under detuning condition. In their experiment, the threshold of two-photon luminescence is about 0.1 TW/cm². In this study, according to the pulse duration, the repetition frequency of the laser, and the size of excitation light spot, it can be calculated that the TPPL threshold is about 0.22 TW/cm², which is in the same order of magnitude with the threshold reported by Dong et al. Considering that the efficiency of three-photon absorption is about one order lower than that of two-photon absorption in the same material, we believe that the crownlike ZnO should have higher three-photon absorption efficiency than Dong's nanowires. According to Mavi et al. [39], the large nonlinear optics effect in nanocrystal is attributed to a large charge density gradient of the crystal interface, which is related to the nanocrystal aspect ratio. In our experiment, the special morphology of the ZnO crystal and the small steps on the shaft can efficiently increase the surface of the crystal. Therefore, the large three-photon effect in crownlike ZnO can be attributed to its large aspect ratio.

Conclusion

In conclusion, the crownlike ZnO crystal was prepared by vapor-phase transport method. Based on V–L–S and V–S

mechanism, the growth model of the crownlike ZnO was proposed. The hexagram cross section of the shaft was attributed to a more rapid growth velocity along $\langle 10\bar{1}0 \rangle$ relative to $\langle 11\bar{2}0 \rangle$ because of a higher supersaturation ratio, and the steplike figuration was believed to be resulting from the shaft transverse growth controlled by V–S mechanism. The disklike cap formation was assigned to the reduction of the catalyst curvature, which resulted in the stop of the shaft growth along [0001] and a longer-time lateral growth of the shaft top due to the diffusion of growth units. Under the excitation of the infrared femtosecond pulse laser, the strong UV TPPL and SHG signals were obtained. The UV spectra and the linear relationship between emission intensity and cube of the excitation power clearly demonstrated TPPL process generated in crownlike ZnO.

Acknowledgments This study was supported by the NSFC (60725413), 973 program (2007CB936300), Natural Science Foundation of Educational Commission of Anhui Province of China (KJ2010A306).

References

- Wu JJ, Liu SC (2002) *J Phys Chem B* 106:9546
- Juárez BH, García PD, Golmayo D, Blanco A, López C (2005) *Adv Mater* 17:2761
- Liu ZW, Yeo SW, Ong CK (2007) *J Mater Sci* 42:6489. doi:[10.1007/s10853-007-1557-2](https://doi.org/10.1007/s10853-007-1557-2)
- Liu B, Zeng HC (2003) *J Am Chem Soc* 125:4430
- Ohara S, Mousavand T, Sasaki T, Umetsu M, Naka T, Adscharit T (2008) *J Mater Sci* 43:2393. doi:[10.1007/s10853-007-1823-3](https://doi.org/10.1007/s10853-007-1823-3)
- Song T, Choung JW, Park J, Park WI, Rogers JA, Paik U (2008) *Adv Mater* 20:4464
- Park WI, Kim DH, Jung SW, Yi G (2002) *Appl Phys Lett* 80:4232
- Chander R, Raychaudhuri AK (2006) *J Mater Sci* 41:3623. doi:[10.1007/s10853-006-6218-3](https://doi.org/10.1007/s10853-006-6218-3)
- Huang MH, Mao S, Feick H, Yan H, Wu Y, Kind H, Weber E, Russo R, Yang P (2001) *Science* 292:1897
- Dem'yanets LN, Li L, Uvarova T, Mininzon Y (2008) *J Mater Sci* 43:2143. doi:[10.1007/s10853-007-2019-6](https://doi.org/10.1007/s10853-007-2019-6)
- Arnold M, Avouris P, Wan PZ, Wang ZL (2002) *J Phys Chem B* 107:659
- Chu XF, Jiang DL, Aleksandra BD, Yu HL (2005) *Chem Phys Lett* 401:426
- Xu J, Chen Y, Li Y, Shen J (2005) *J Mater Sci* 40:2919. doi:[10.1007/s10853-005-2435-4](https://doi.org/10.1007/s10853-005-2435-4)
- Wang ZL, Song JH (2006) *Science* 312:242
- Wang G, Kiehne GT, Wong GKL, Kettersson JB, Liu X, Chang RH (2002) *Appl Phys Lett* 80:401
- Neumann U, Grunwald R, Griebner U, Steinmeyer G, Seeber W (2004) *Appl Phys Lett* 84:170
- Petrov GI, Shchelavskiy V, Yakovlev VV, Ozerov I, Chelnokov E, Marine W (2003) *Appl Phys Lett* 83:3993
- Zhang CF, Dong ZW, You GJ, Qian SX, Deng H, Gao H, Yang LP, Li Y (2005) *Appl Phys Lett* 87:051920
- Zhang CF, Dong ZW, You GJ, Qian SX, Deng H, Wang JC (2006) *Appl Phys Lett* 89:042117
- Tuff LW, Boggess TF (1993) *Prog Quant Electron* 17:299
- Henari FZ, Morgenstern K, Blau WJ (1995) *Appl Phys Lett* 67:323
- Chon JWM, Zijlstra P, Gu M, Embden JV, Mulvaney P (2004) *Appl Phys Lett* 85:5514
- Xu CX, Sun XW, Dong ZL, Yu MB (2004) *Appl Phys Lett* 85:3878
- Lao JY, Huang JY, Wang DZ, Ren ZF (2003) *Nano Lett* 3:235
- Zhang XG, Zhang Y, Xu J, Wang Z, Chen XH, Yu DP, Zhang P, Qi HH, Tian Y (2005) *Appl Phys Lett* 87:123111
- Hu JQ, Li Q, Wong NB, Lee CS, Lee ST (2002) *Chem Mater* 14:121
- Hu PA, Liu YQ, Wang XB, Fu L, Zhu DB (2003) *Chem Commun* 11:1304
- Wang FF, Cao L, Pan AL, Liu RB, Wang X, Zhu X, Wang SQ, Zou BS (2007) *J Phys Chem C* 111:7655
- Xiao J, Zhang XX, Zhang GM (2008) *Nanotechnology* 19:295706
- Jayakumar OD, Sudarsan V, Sudakar C, Naik R, Vatsa RK, Tyagi AK (2010) *Scripta Mater* 62:662
- Djurišić AB, Choy WCH, Roy VAL, Leung YH, Kwong CY, Cheah KW, Rao TG, Chan WK, Lui HF, Surya C (2004) *Adv Funct Mater* 14:856
- Vanheusden K, Seager CH, Warren WL, Tallant DR, Voigt JA (1996) *Appl Phys Lett* 68:403
- Garces NY, Wang L, Bai L, Giles NC, Halliburton LE, Cantwell G (2002) *Appl Phys Lett* 81:622
- Lin B, Fu Z, Jia Y (2001) *Appl Phys Lett* 79:943
- Studenikin SA, Cocivera M (2002) *J Appl Phys* 91:5060
- Ghosh A, Deshpande NG, Gudage YG, Joshi RA, Sagade AA, Phase DM, Sharma R (2009) *J Alloys Compd* 469:56
- Yee JH (1972) *Phys Rev B* 5:449
- Dong ZW, Zhang CF, Liu KJ, Yan YL, Qian SX (2007) *Proc SPIE* 6839:68390h
- Mavi HS, Prusty S, Shukla AK, Abbi SC (2003) *Opt Commun* 226:405